https://doi.org/10.3311/PPCi.45225
Creative Commons Attribution

Periodica Polytechnica Civil Engineering

Seismic Vulnerability and Damage Mechanisms of a Historic Masonry Complex: Numerical Assessment and Validation Against Observed Earthquake Damage

Şahin Sözen[1*]

[1] Tokat Gaziosmanpasa University, Faculty of Engineering and Architecture, Department of Civil Engineering, Taşlıçiftlik Kampüsü 60150, Tokat, Türkiye
[*] Corresponding author, e-mail: sahin.sozen@gop.edu.tr

Received: 22 June 2026, Accepted: 15 October 2026, Published online: 17 November 2026

Abstract

The preservation of historic buildings that constitute an important part of the world's cultural heritage requires reliable prediction of their structural behavior under seismic loading. In this study, the seismic behavior and structural vulnerability of the historic Amasya Çilehane Complex are investigated using finite element-based modal analysis, nonlinear static analysis, and nonlinear time-history simulations. The base-shear-to-weight ratio associated with the approximate onset of nonlinear response ranged from 0.23 to 0.46 for the selected ground motions. Although the calculated global drift ratios remained relatively low, the nonlinear analyses revealed localized tensile-strength exceedance and residual strain concentrations, particularly around façade openings, dome-support transition zones, and interior masonry walls. These results indicate that significant local damage may develop before substantial global deformation occurs. Comparison of the numerically identified critical regions with crack patterns documented in archival photographs showed notable spatial consistency, providing qualitative corroboration of the predicted damage mechanisms. Overall, the findings demonstrate the high seismic vulnerability of the complex and provide a rational basis for identifying critical structural regions and guiding future evaluations of conservation-compatible strengthening alternatives.

Keywords

seismic vulnerability, historic masonry structures, nonlinear time-history analysis, finite element modeling, earthquake damage mechanisms

1 Introduction

Until the invention of modern building materials such as steel and reinforced concrete, buildings were primarily constructed of masonry. Many structures registered as historical buildings were constructed using this technique; however, despite their adequate performance under gravity loads, they are highly vulnerable to seismic actions due to their very limited tensile strength, energy dissipation capacity, and ductility, and may suffer severe damage or even complete collapse during moderate earthquakes [1–8]. In addition, problems in the joints of structural elements, inadequate out-of-plane bearing capacity of masonry walls, and deterioration of structural materials further increase the vulnerability of masonry buildings to earthquakes [7]. The preservation of historic buildings is crucial not only for transmitting cultural heritage to future generations but also for developing and maintaining a country's tourism potential. Protecting historic buildings from destructive impacts, a common goal of almost all societies, depends on determining their mechanical behavior and, accordingly, their performance, especially in future earthquakes. It is difficult to determine the mechanical behavior of places of worship, which occupy an important place in the historic building stock and generally have complex geometric shapes. Additionally, the different material properties and construction techniques used in these buildings make it challenging to determine their structural behavior, especially under lateral loads. Fortunately, with current engineering capabilities, it is possible to determine the mechanical behavior of structures in future earthquakes and the potential damage and thus take the necessary protective measures.

Türkiye is located on several active fault systems associated with the North Anatolian Fault Zone and the East Anatolian Fault Zone, making the country highly suscep-

Cite this article as: Sözen, S. "Seismic Vulnerability and Damage Mechanisms of a Historic Masonry Complex: Numerical Assessment and Validation Against Observed Earthquake Damage", Periodica Polytechnica Civil Engineering, 2026. https://doi.org/10.3311/PPCi.45225

tible to destructive earthquakes. Due to its seismically active geology, Türkiye has experienced 21 devastating earthquakes with a magnitude over 7 in the past century. Most recently, two major earthquakes occurred 13 hours apart in 2023, severely affecting 11 cities in Türkiye (Pazarcık/Kahramanmaraş M_w = 7.7 and Elbistan/Kahramanmaraş M_w = 7.6) [9]. Fig. 1 [9, 10] shows the earthquake hazard map of Türkiye and the earthquakes that have occurred in the last century. Not only in Türkiye, but also in other European countries with rich histories, historical buildings are known to be vulnerable to earthquakes due to high seismic risk. The most effective way to preserve historic buildings is to predict their structural behavior in advance. It is also possible to take protective measures for a historic building if its response to a potential earthquake can be realistically calculated. In the literature, many studies address the response of historic buildings to seismic actions [6–8, 11–15].

Kocaman and Kazaz [7] investigated the seismic behavior of four historical mosques in Türkiye. In the study, the damage propagation and collapse mechanism of the mosques were investigated by detailed finite element models. Nonlinear time-history analyzes were carried out using the acceleration records of the Erzincan 1992, Cape Mendocino 1992 and Kobe 1995 earthquakes. Kocaman and Kazaz [7] concluded that the crack distribution and collapse mechanism of square-plan masonry dome mosques can be generalized. Gonçalves et al. [16] investigated the performance of existing masonry buildings through static pushover analyzes. They compared the Finite Element Method (FEM) and the Equivalent Frame Method (EFM) to validate the chosen input parameters. Dedeoğlu et al. [14] investigated the effects of a 5.9 magnitude earthquake in November 2022 in Türkiye on masonry buildings in rural areas. In the first part of the study, the tectonic features of the North Anatolian fault line, the seismic features of the earthquake zone and the main shock are presented. The second part, on the other hand, presents the responses of masonry buildings in rural areas to the earthquake and the main causes of damage. Finally, some retrofitting techniques to improve the seismic performance of existing masonry buildings are presented. Cakir et al. [8] conducted a performance-based assessment of a historic masonry mosque built in the early Ottoman Empire. The study, which includes a structural system investigation, damage assessment studies, seismicity of the region, geotechnical field tests, geotechnical laboratory tests, ambient vibration tests (AVTs) and finite element analyzes, provides essential recommendations for the protection of the Şerafettin Mosque in Türkiye. Şentürk et al. [6] investigated the effects of different strengthening methods for earthquake-damaged historic masonry buildings. In the study, the earthquake behavior of Alaeddin Bey Mosque in Türkiye is determined by time-history analysis considering the acceleration data of Erzincan, Kocaeli and Van earthquakes. According to the results of the analysis, it is recommended to reinforce the damaged parts of the minaret with CFRP fabric and steel plates. The effectiveness of the retrofit is discussed in detail in the study. Onat et al. [17] investigated in detail the seismic behavior of the historical Ak Minaret Mosque in Malatya, the damage limits, the reason for unexpectedly lower damage

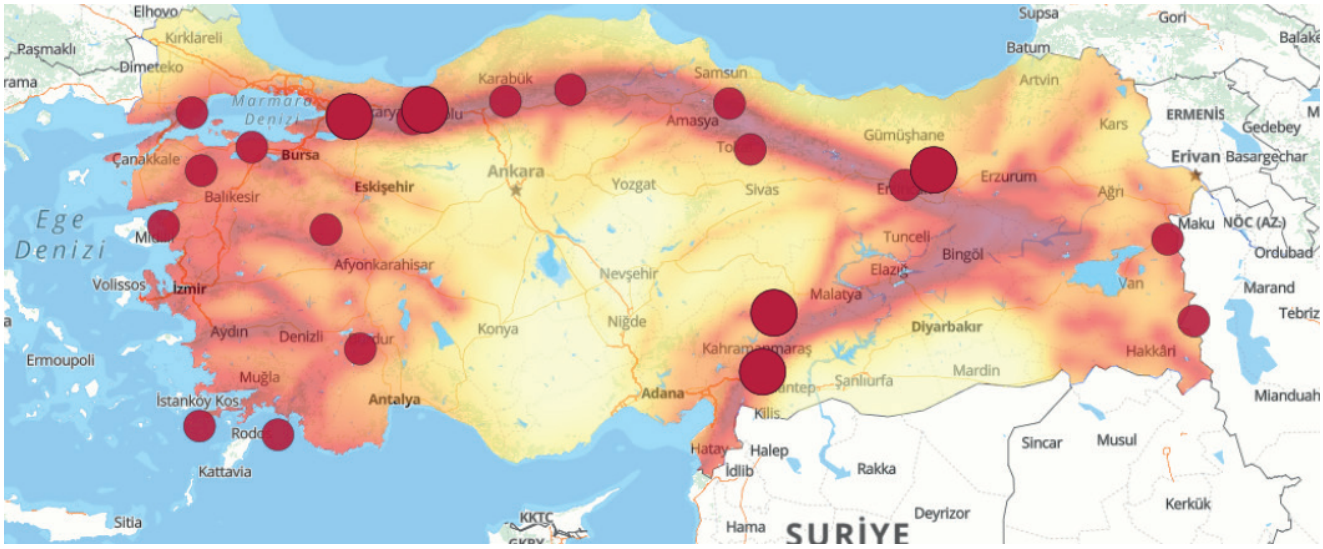


Fig. 1 Earthquake locations with magnitudes over 7 in the last century [9, 10]

due to earthquakes, the potential damage mode and possible resistive earthquake loads by creating and analyzing a finite element model based on the dynamic properties of the mosque determined before the Kahramanmaraş earthquake in Türkiye. Although many studies have analyzed the seismic response of historic masonry structures using numerical methods, relatively few studies have attempted to validate numerical damage predictions through comparison with damage observed after real earthquakes.

Several methods have been developed and applied in recent decades for the seismic assessment of masonry structures, each with specific advantages and limitations. The discrete macro-element method is the most popular, as it can capture the global mechanical behavior and collapse mechanisms with little computational effort, making it suitable for large-scale vulnerability assessments [18, 19]. In contrast, hybrid experimental–numerical methods combine laboratory tests with numerical modeling. They can thus estimate more realistic nonlinear behavior, although they require specialized equipment and may be limited by experimental constraints [20]. Probabilistic fragility assessments, on the other hand, provide a statistical framework to quantify the probability of damage states under seismic loading and thus support risk-informed decision making; however, their accuracy is highly dependent on the availability of representative structural data and ground motion records [21]. Overall, these approaches are complementary rather than mutually exclusive, and the choice among them often reflects the trade-off between accuracy, generality, and resource availability.

In this study, the seismic performance of the historic Amasya Çilehane Complex is evaluated using nonlinear time-history analyses based on the finite element method (FEM) and real earthquake records. The main objective is to assess the seismic vulnerability of the structure and to identify its dominant damage mechanisms through detailed nonlinear numerical simulations. Particular emphasis is placed on comparing the numerically predicted damage zones with crack patterns documented after past earthquakes, thereby providing qualitative corroboration of the adopted numerical modeling strategy. Based on these analyses, the potential damage mechanisms of the structure are interpreted and compared with archival photographic evidence of past earthquake damage. In addition, the implications of the identified damage mechanisms for future conservation-compatible strengthening studies are discussed.

2 Çilehane complex

The Çilehane Complex in Amasya is an important historical and religious building from the Ottoman period. The complex takes its name from the rooms where dervishes retreat and focus on their spiritual journey. Such buildings typically served as *Sufi* training centers and included structures with various religious and social functions, such as mosques, madrasas, mausoleums, tombs, and fountains. The location of the complex in Amasya and the layout of the buildings are given in Fig. 2.

One of the most remarkable parts of the complex is the small rooms, called Çilehane in Turkish. These rooms are where dervishes retreat, worship, and receive spiritual training. The rooms are generally designed to admit very little light, allowing the dervishes to withdraw from the world and embark on an inner journey. The mosque and the madrasa are also important parts of the complex. The mosque serves as the worship center and was built in classical Ottoman architectural style. *The madrasa* was used as an institution for religious education. The building, which has a square floor plan, measures 25.31 m by 23.55 m. While

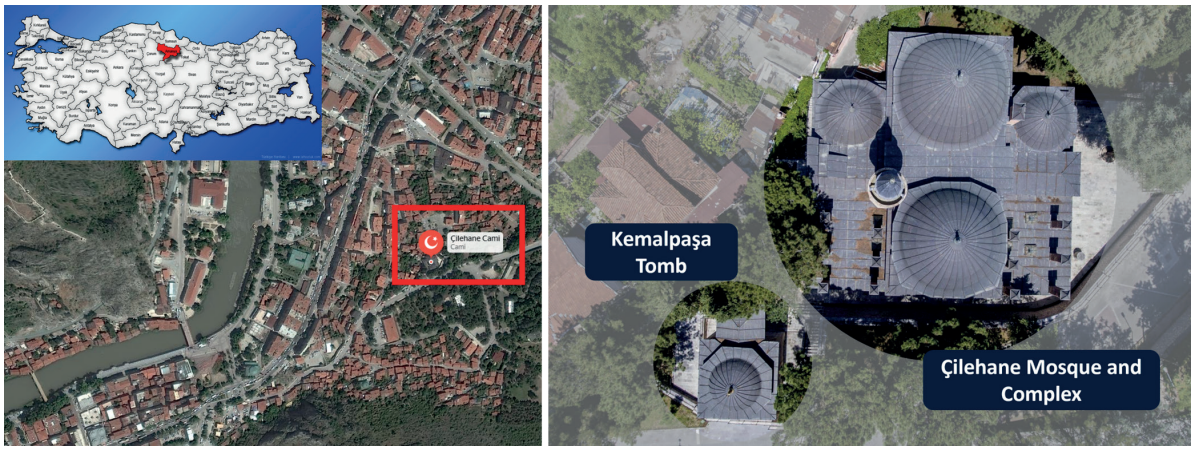


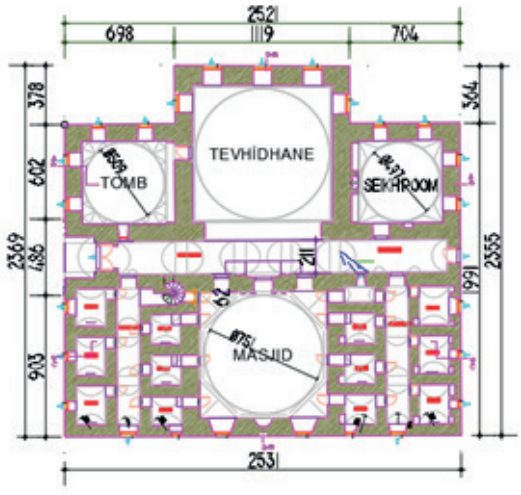
Fig. 2 The location of the complex

the ordeal rooms are covered with vaults, the tevhidhane, the masjid, the sheikh's room, and the burial chambers are covered with four domes with diameters ranging from 9 m to 5 m (Fig. 3).

The Çilehane Mosque and its complex were built in 1413 by Yakup Pasha, one of the emirs of Çelebi Mehmet who is the fifth sultan of the Ottoman Empire. The building, now used as a mosque, was originally a Halveti tekke. It consists of a lodge, a masjid, and ordeal cells. Near the western entrance is a domed structure considered a burial place. The walls are built of quarry stones filled with red mortar, supported by two rows of horizontally laid bricks. The masonry of the Çilehane complex was built using a single-layer system and consists of large stone blocks approximately 60–80 cm thick. The average stone size ranges from 25 to 40 cm, and the blocks are generally roughly hewn and laid without a regular horizontal course. Decorative horizontal courses of red bricks are used in some areas within the masonry. In such single-layer systems, load-bearing behavior relies primarily on the interlocking of the stone blocks under pressure, with the lime mortar providing limited binding strength. While sufficient compressive strength is achieved under vertical loads, lateral loads tend to cause shear cracks, joint openings, and relative displacements between the stones or bricks.



(a)



(b)

Fig. 3 Plans of the Çilehane Complex (a) Layout plan; (b) Floor plan

The mosque is entered through an arched doorway that leads to a space known as an eyvan in Turkish. An eyvan is an architectural unit constructed of cut stone, usually covered with a vault, enclosed on three sides, and completely open on one side. The windows that illuminate the interior are framed in marble and have brick arches. Upon entering through the west door, small passageways on the right lead to the prayer room and seclusion rooms, while on the left are the tomb and tekke. A large dome covers both the mosque and the tekke. The 1939 Erzincan earthquake severely damaged the Çilehane, and the General Directorate of Foundations carried out restoration work in 1964 and 2020 [22].

The Çilehane Complex, open to visitors, is preserved today as a historical and cultural heritage site. Additionally, the complex is surrounded by Amasya's natural beauty, offering visitors both spiritual and aesthetic experiences. A current photograph of the complex and the Çile rooms are shown in Fig. 4 [23].



(a)



(b)



(c)

Fig. 4 Interior view of the retreat rooms in the complex [23] (a) Current photo of the complex; (b) Retreat (*in Turkish Çile*) rooms; (c) A view from inside the rooms

3 Modelling strategy and structural analyses

It is essential to determine the structural behavior of historic buildings with sufficient accuracy to assess whether retrofitting is necessary. However, conducting the studies required to determine structural behavior using a classical engineering approach is almost impossible. The finite element method and computers now make it possible to model historic structures and analyze these models under different loading conditions, allowing us to solve complex engineering problems. Although macro-element and equivalent frame models remain popular for the global seismic assessment of masonry buildings, recent research has further developed these approaches. Decret et al. [24] presented a new finite element macro model capable of simulating the in-plane cyclic behavior of unreinforced masonry with a limited number of degrees of freedom, enabling efficient calculation with reliable accuracy. Furthermore, Prosperi et al. [25] conducted a systematic comparison between macro modeling and simplified micro modeling strategies. They found that macro models using the Engineering Masonry Model can predict damage severity with an accuracy of about 10% compared to experimental results and are significantly more computationally efficient than micromodels. These advances reinforce the validity of using a 3D finite element continuum approach in ANSYS [26], especially when a detailed representation of complex geometries and localized damage patterns is required, despite higher computational requirements and calibration effort. Thus, ANSYS Workbench [26] software was used for the analysis in this study.

3.1 Finite element model

A detailed finite element model of the complex was constructed using SolidWorks [27]. Drawings obtained from the General Directorate of Foundations DGF [28] were used to create the numerical model. Fine architectural details such as decorative elements, small ornaments, and minor façade features were not included in the numerical model because their contribution to the global structural response is negligible. After the complex was modeled in the SolidWorks environment, it was transferred to ANSYS [26] software and then meshed. In the numerical model, soil-structure interaction (SSI) was not considered because detailed geotechnical information about the foundation soil and boundary conditions was unavailable. Instead, the foundation of the structure was assumed to be fixed, which is a conservative approach for analyzing such cases when site-specific information is lacking. While not considering SSI may slightly overestimate stiffness and underestimate displacement, this simplification provides a reasonable and computationally efficient simulation of the global structural response. In the future, it will be possible to include SSI effects when sufficient soil properties and subsoil investigation data are available. Fixed support is widely preferred in studies where the soil-structure interaction is not considered. Masonry minarets are slender structural components with dynamic characteristics and collapse mechanisms that may differ substantially from those of the adjoining main building [6, 29]. Accordingly, the present numerical investigation was restricted to the main masonry complex, and the minaret was excluded from the finite element model. Therefore, the modal properties, participating masses, base-shear response, and damage mechanisms reported in this study refer specifically to the modeled main structural system excluding the minaret. The seismic response and local collapse mechanism of the minaret require a separate or explicitly coupled numerical assessment and are outside the scope of the present study.

The finite element model is shown in Fig. 5. The numerical model consists of 184464 nodes and 107504 finite elements.

The Solid65 element from the ANSYS [26] element library was used for the finite element model, as it has been proven to be able to represent the nonlinear behavior of brittle materials such as masonry and concrete. This three-dimensional element consists of eight nodes, each with three translational degrees of freedom, as shown in Fig. 6(a). Solid65 is able to simulate key material failure mechanisms, including tensile cracking, compressive crushing, and plastic deformation, making it particularly

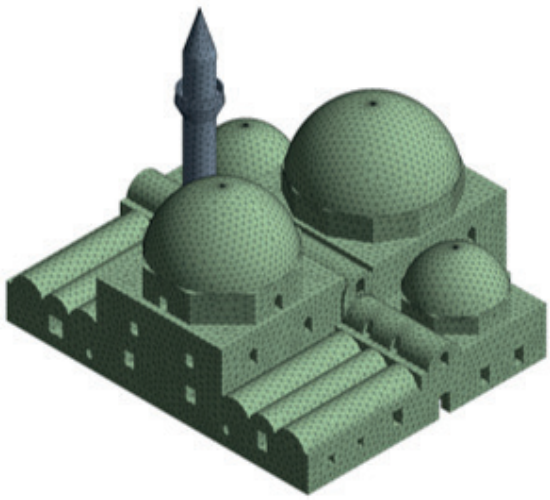


Fig. 5 Solid models of the complex

suitable for capturing the structural response of historic masonry walls under seismic loading. The material is assumed to be isotropic before cracking, with cracking allowed in three orthogonal directions at each integration point. Once a crack occurs, the smeared crack approach is applied, representing the effect of localized damage by altered material properties rather than discrete discontinuities. The corresponding stress-strain behavior of a cracked section is shown in Fig. 6(b).

Regarding mesh discretization, both the shape and size of the elements were determined according to established criteria for numerical modeling. Where the geometry allowed, a structured mesh of hexahedral elements was used, as this configuration is known to minimize numerical errors and ensure stable convergence. The element size was determined by a mesh sensitivity study, which found a balance between computational efficiency and accuracy. In particular, a finer mesh was used in regions where stress concentrations are expected (e.g., openings), while relatively coarser elements were used in less critical areas. This strategy ensured that the numerical model could reliably capture local nonlinearities without incurring excessive computational costs.

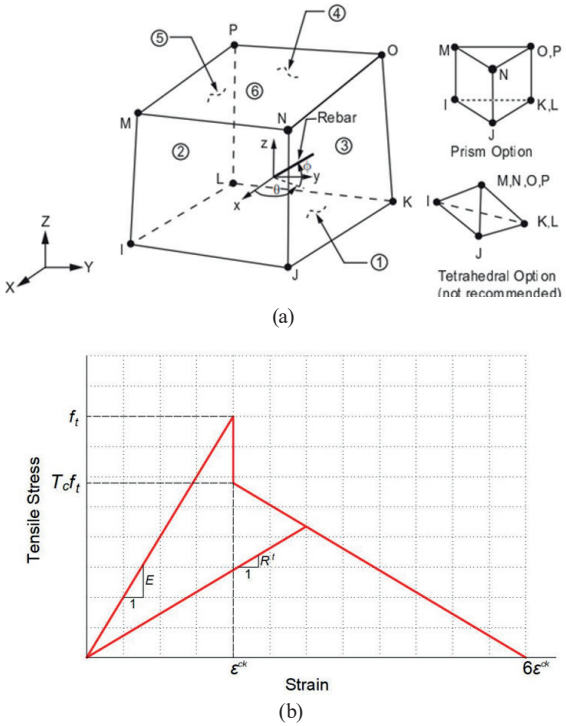


Fig. 6 Solid element used in analyses and material model (a) Solid 65 geometry [26]; (b) Material model

3.2 Material model and properties

The five-parameter Willam–Warnke model [30] was adopted to represent the nonlinear behavior of the masonry material. Although the model was originally developed for homogeneous and isotropic materials such as concrete, numerous studies have successfully applied it to describe the macro-level nonlinear behavior of heterogeneous materials, including masonry walls and stone structures [31–33]. In such applications, masonry is represented as an equivalent continuum characterized by its average mechanical properties rather than by explicitly modelling its individual stone, brick, and mortar components. The constitutive parameters may be calibrated using experimental data when structure-specific test results are available; alternatively, representative mechanical properties reported for comparable masonry typologies may be adopted when experimental characterization is not feasible. Therefore, the use of the Willam–Warnke model in the present study is consistent with modelling approaches previously employed for the nonlinear analysis of historic masonry structures.

Recent experimental–numerical benchmark studies have further demonstrated both the capabilities and limitations of continuum finite element approaches for the nonlinear seismic analysis of masonry structures. Aşıkoğlu et al. [34] compared a three-dimensional continuum finite element model with shaking-table tests conducted on a half-scale stone masonry building aggregate and showed that, following calibration of material and interface parameters, the numerical model provided reasonable predictions of base shear, displacement response, and damage patterns. Bianchini et al. [35] similarly employed three-dimensional macro finite element models to reproduce the nonlinear dynamic response of the same experimentally tested stone masonry aggregate, highlighting the importance of material calibration and an appropriate representation of structural connections. In addition, Xie et al. [36] compared nonlinear finite element predictions with shaking-table results for a scaled historical masonry tower and reported satisfactory agreement in dynamic response and failure mechanisms. These studies support the applicability of continuum-based nonlinear modelling for masonry structures while also emphasizing that the predictive accuracy of such models is strongly dependent on material characterization, constitutive assumptions, and model calibration. Accordingly, these experimental benchmarks provide methodological support for the modelling framework adopted herein, but they should not be interpreted as direct validation of the specific material parameters used for the Çilehane Complex.

The model parameters (f_t, f_c, f_{cb}, σ_h^a, f_1 and f_2) represent the ultimate uniaxial tensile strength, ultimate uniaxial compressive strength, ultimate biaxial compressive strength, ambient hydrostatic stress state, ultimate compressive strength for a state of biaxial compression superimposed on hydrostatic stress state σ_h^a, ultimate compressive strength for a state of uniaxial compression superimposed on hydrostatic stress state σ_h^a, respectively. In the adopted formulation, the failure surface is primarily governed by the uniaxial tensile and compressive strengths, while the remaining parameters are derived from these strength values as follows [30]:

$$f_{cb} = 1.2 f_c, \quad f_1 = 1.45 f_c, \quad f_2 = 1.725 f_c, \quad \sigma_h^a = \sqrt[3]{f_c} \qquad (1)$$

The uniaxial stress–strain relationship adopted for the material model is shown in Fig. 7.

The mechanical properties used in the numerical model were adopted from the literature because structure-specific in-situ or laboratory testing could not be performed due to conservation constraints associated with the protected status of the Çilehane Complex. The selected properties were based on studies investigating historic masonry structures with comparable material characteristics, construction techniques, and structural typologies. Accordingly, the adopted values should be regarded as representative literature-based properties rather than experimentally calibrated parameters specific to the Çilehane Complex. Previous studies on comparable masonry structures report compressive strengths ranging approximately from 1.80 to 5.00 MPa and elastic modulus from 430 to 8500 MPa [37–40]. Considering these reported ranges and the characteristics of the masonry system investigated in the present study, a compressive strength of 4.50 MPa and an elastic modulus of 3900 MPa were adopted. The tensile strength and Poisson's ratio were taken as 0.30 MPa and 0.20, respectively, based on representative values reported and adopted for comparable historic masonry typologies in the cited literature. The density of the masonry was taken as 2650 kg/m³. The resulting mechanical properties used in the numerical model are summarized in Table 1. It should be emphasized that the absence of structure-specific mechanical testing introduces uncertainty into the quantitative nonlinear response predicted by the numerical model, particularly with respect to stress magnitude, strain demand, and damage initiation. This limitation is explicitly considered when interpreting the numerical results and is further discussed in Section 4.3. Accordingly, the comparison between the numerically predicted critical regions and historically documented earthquake damage is used as qualitative corroboration of the predicted damage mechanisms rather than as a substitute for structure-specific experimental calibration.

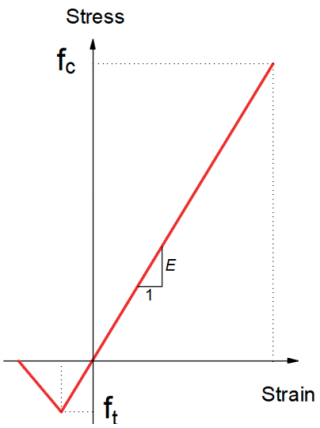


Fig. 7 Uniaxial stress-strain relationship of the material

Table 1 Material properties adopted from literature sources

Tensile Strength, f_t (MPa)	Compressive Strength, f_c (MPa)	Density, ρ (kg/m³)	Poisson's ratio υ	Modulus of elasticity, E (MPa)
0.3	4.5	2650	0.20	3900

3.3 Mesh sensitivity analysis

Due to the large scale and geometric complexity of the finite element model, a mesh sensitivity analysis was performed to evaluate the influence of spatial discretization on both the global dynamic characteristics and the nonlinear seismic response of the structure. Three mesh configurations with global average element sizes of 750 mm (coarse), 500 mm (medium), and 350 mm (fine) were considered. The corresponding models consisted of 46194, 107504, and 255183 finite elements, respectively.

As a first stage, the influence of mesh refinement on the global stiffness characteristics was evaluated through prestressed modal analyses. The eigenvalue analyses were performed about the nonlinear equilibrium state obtained after application of the gravity preload, using identical material properties and boundary conditions for all mesh configurations. The fundamental frequencies obtained for the coarse, medium, and fine meshes were 10.666, 10.557, and 10.505 Hz, respectively. Taking the fine-mesh solution as the reference, the corresponding differences were 1.53% and 0.49% for the coarse and medium meshes. The small difference between the medium and fine meshes indicates that further refinement beyond the 500 mm discretization has only a limited influence on the predicted global stiffness characteristics.

To extend the mesh sensitivity assessment to the nonlinear seismic response, additional nonlinear time-history analyses were conducted for all three mesh configurations. The spectrally matched E–W and N–S components of the 1992 Erzincan earthquake were applied simultaneously. The same constitutive model, material parameters, damping ratio, boundary conditions, ground-motion input, and nonlinear analysis procedure were adopted for all three models. For the fine-mesh model, the time-stepping parameters were adjusted to obtain a stable converged solution because the settings used for the coarser meshes did not provide numerical convergence. This adjustment was limited to numerical solution control, while the physical, material, boundary, and loading assumptions remained unchanged.

The sensitivity of the global nonlinear response was evaluated using the peak total base shear, V_{max}, and the maximum total deformation at the dome-tip control point, u_{max}. As summarized in Table 2, the peak total base-shear values were 27011, 26956, and 26932 kN for the coarse, medium, and fine meshes, respectively. Relative to the fine-mesh solution, the corresponding differences were only 0.29% and 0.09% for the coarse and medium meshes. The maximum dome-tip deformations were 2.4767, 2.6411, and 2.7001 mm, resulting in differences of 8.27% and 2.19% for the coarse and medium meshes, respectively. The peak base-shear responses occurred at approximately 2.84 s, while the maximum dome-tip deformations occurred at approximately 2.92 s for all three mesh configurations. Thus, although the deformation response exhibited greater sensitivity to mesh refinement than the global force response, the difference decreased substantially between the medium and fine discretizations.

To additionally evaluate the sensitivity of the predicted local tensile response, the maximum principal tensile stress envelopes over the entire ground-motion duration were compared for the three mesh configurations (Fig. 8). The maximum principal stress values were 0.47003, 0.45773, and 0.44416 MPa for the coarse, medium, and fine meshes, respectively. Relative to the fine-mesh result, the differences were 5.82% for the coarse mesh and 3.06%

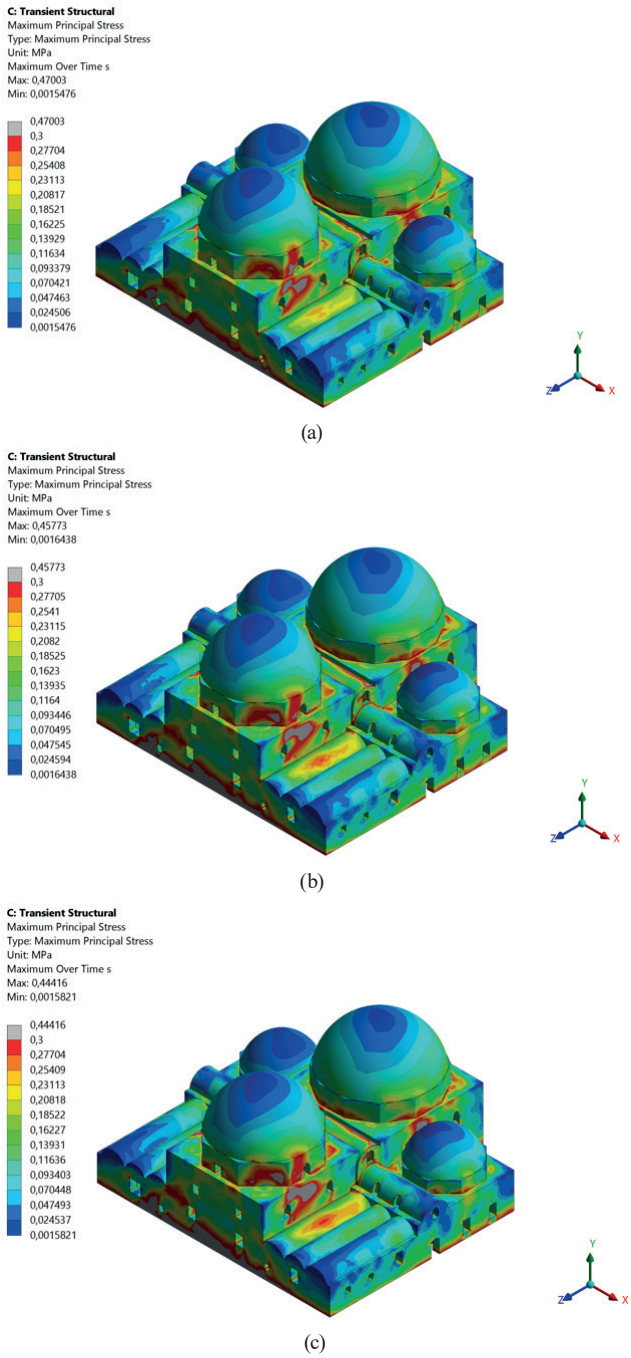


Fig. 8 Maximum principal tensile stress envelopes obtained from the nonlinear time-history analyses using the spectrally matched Erzincan earthquake record: (a) 750 mm coarse mesh; (b) 500 mm medium mesh; (c) 350 mm fine mesh

Table 2 Mesh sensitivity results based on pre-stressed modal and nonlinear time-history analyses

Mesh type	Average element size (mm)	Number of elements	Fundamental frequency f_1 (Hz)	Δf* (%)	Peak Base Shear (kN)	ΔV* (%)	Max. Dome Tip Deformation (mm)	Δu* (%)	$\sigma_{1,max}$ (MPa)	$\Delta\sigma_1$ (%)
Coarse	750	46194	10.666	1.53	27011	0.29	2.4767	8.27	0.470	5.82
Medium	500	107504	10.557	0.49	26956	0.09	2.6411	2.19	0.457	3.06
Fine	350	255183	10.505	0.00	26932	0.00	2.7001	0.00	0.444	0.00

*Δf, ΔV, Δu and $\Delta\sigma_1$ denote the absolute percentage differences relative to the corresponding results obtained from the fine-mesh configuration.

for the medium mesh. In all three models, the maximum principal tensile stress exceeded the adopted masonry tensile strength of 0.30 MPa. More importantly, the spatial distributions of the tensile stress concentrations remained consistent with mesh refinement, with the principal high-demand regions repeatedly occurring around façade openings, dome-support transition zones, and critical wall regions. Therefore, although the magnitude of the local peak tensile stress exhibited some mesh sensitivity, the predicted localization of the critical tensile-demand regions remained stable among the three discretizations.

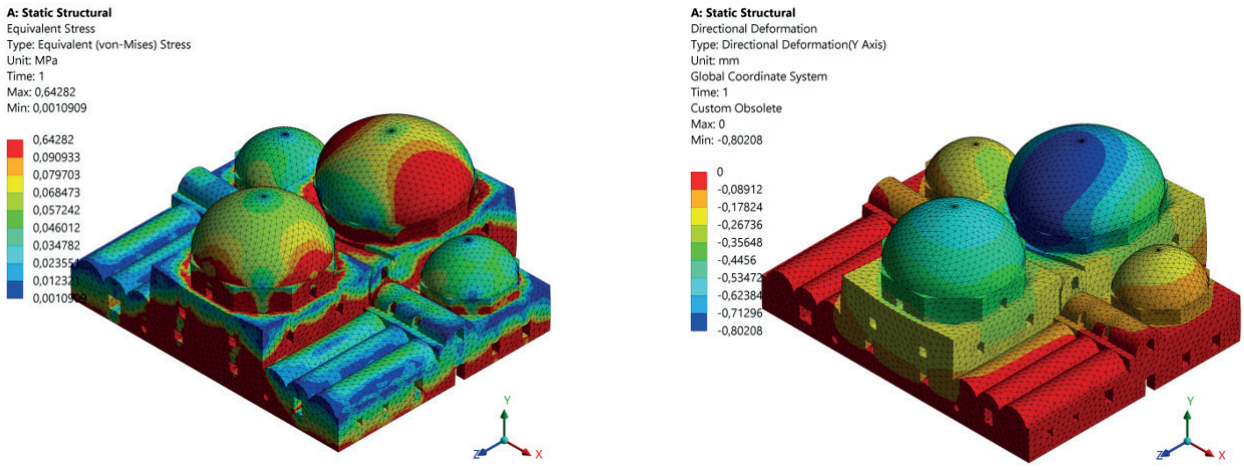
Overall, the modal, global nonlinear, and local tensile-response comparisons indicate that the numerical response becomes substantially more stable when the mesh is refined from the medium to the fine discretization. The differences between the 500 and 350 mm meshes were limited to 0.49% in fundamental frequency, 0.09% in peak total base shear, 2.19% in maximum dome-tip deformation, and 3.06% in maximum principal tensile stress. Considering these differences together with the substantially greater computational demand of the fine-mesh model, the 500 mm mesh was retained for the principal structural analyses as an appropriate balance between numerical accuracy and computational efficiency. Accordingly, the results indicate limited sensitivity of both the global nonlinear response and the predicted localization of critical tensile-demand regions to further mesh refinement beyond the medium discretization.

3.4 Nonlinear static analysis under gravity load

Historic masonry buildings generally do not present any risk due to their own weight. However, a non-linear static analysis under self-weight was conducted to identify areas where stresses and deformations accumulate. Geometric and material non-linearity are taken into account in the analysis. When examining the von Mises stress distribution obtained from the non-linear static analysis (Fig. 9(a)), it can be seen that the maximum equivalent stress is 0.64 MPa. The maximum stresses occur on the side surfaces of the domes in the east-west direction, on the dodecagonal pulleys connecting the domes to the substructure, and on the north-south walls of the building. Maximum stresses are also observed on the lower parts of the east-west façade walls near the foundation. The stresses are limited in the sections where the ordeal rooms are located. Fig. 9(b) shows that the large dome is subjected to a vertical deformation of 0.80 mm. In the analysis, the total weight of the structure was calculated as 3.2391×10^4 kN.

3.5 Modal analysis

A modal analysis was performed to determine the natural oscillation periods and mode shapes of the structure. The study considered 30 mode shapes, with a focus on eight modes. The mode shapes of the first eight modes are shown in Fig. 10. In the first mode, the building exhibits translational motion in the Z direction. In the second mode, the masses covered with domes move in the opposite north-south direction. In the third and fourth modes, the building exhibits translational movement in the X direction, while in the fourth mode, the main masses move in opposite directions along the east-west axis. The fifth and sixth modes display a linear characteristic as a combination of the previous modes, while the seventh mode exhibits a torsional characteristic. The modal properties and participating mass ratios presented in Table 3 correspond to the modeled main complex excluding the minaret.



(a) (b)

Fig. 9 Stress and deformation distribution under gravity load (a) Von Mises stress (MPa); (b) Directional deformation (mm)

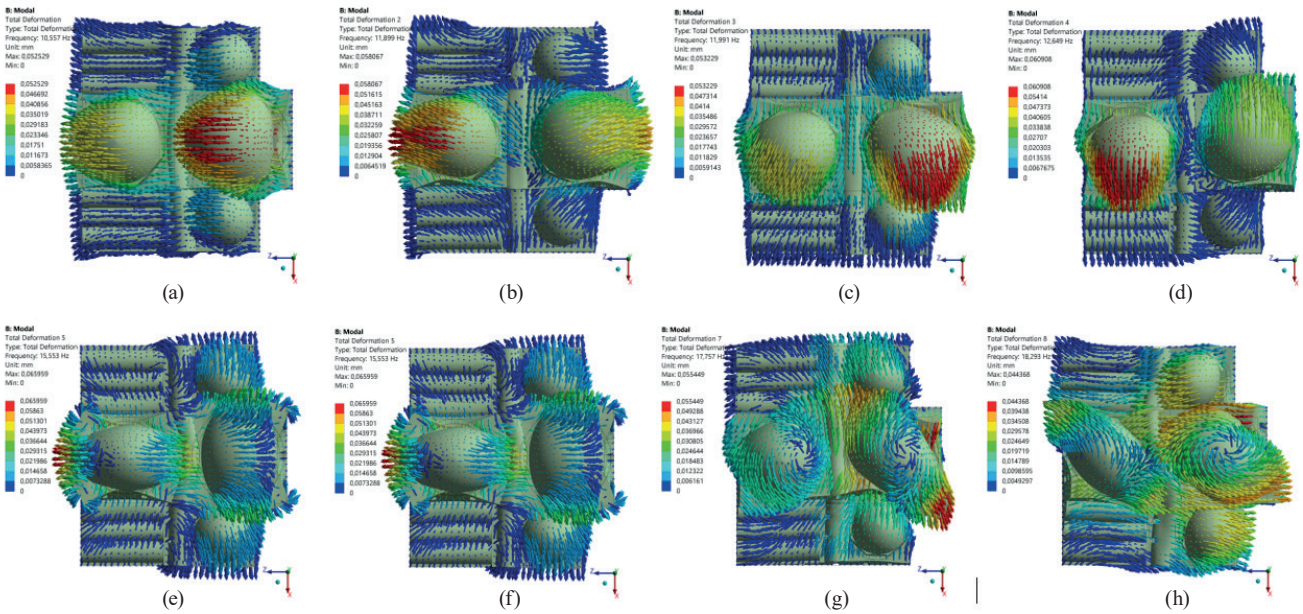


Fig. 10 Vibration mode shapes and frequencies (a) Mode shape 1; (b) Mode shape 2; (c) Mode shape 3; (d) Mode shape 4; (e) Mode shape 5; (f) Mode shape 6; (g) Mode shape 7; (h) Mode shape 8

Table 3 Frequency and modal participation results

Mode	Frequency (Hz)	Participation factor Directions			Cumulative effective mass fraction Directions		
		X	Y	Z	X	Y	Z
1	10.557	0.37598	-0.61028	37.342	6.07E-05	3.21E-04	0.58598
2	11.899	-11.391	0.65093	5.2224	5.58E-02	6.86E-04	0.59744
3	11.991	35.143	3.11E-02	1.3786	0.58653	6.87E-04	0.59824
4	12.649	6.3607	-0.18738	0.71288	0.60392	7.17E-04	0.59845
5	15.553	0.58668	-0.5603	-4.4016	0.60406	9.88E-04	0.60659
6	17.467	-1.209	3.456	-0.55803	0.60469	1.13E-02	0.60672
7	17.757	-9.3072	0.2681	0.73327	0.64192	1.13E-02	0.60695
8	18.293	3.446	1.163	1.3924	0.64702	1.25E-02	0.60776
9	19.871	-0.38052	10.462	11.49	0.64708	0.10683	0.66324
10	20.712	3.9119	-0.29475	-0.35318	0.65366	0.1069	0.6633
11	21.216	-16.325	0.72711	2.8388	0.76818	0.10736	0.66668
12	21.853	1.951	2.5877	22.205	0.76982	0.11313	0.87389
13	21.987	10.784	1.4663	0.85131	0.81979	0.11498	0.8742
14	22.323	0.5984	-9.2033	4.0881	0.81995	0.18798	0.88122
15	22.632	10.919	-0.24663	-0.21148	0.87118	0.18803	0.88124
16	23.639	0.57797	15.394	-9.8217	0.87132	0.39225	0.92178
17	24.702	-4.8319	-2.9913	-0.89505	0.88136	0.39997	0.92212
18	24.983	-2.4948	-8.9761	3.8243	0.88403	0.4694	0.92826
19	25.182	-1.7504	15.864	4.3399	0.88535	0.68629	0.93618
20	25.856	4.3538	-0.92634	4.0094	0.89349	0.68703	0.94293
21	26.247	-0.43067	-6.8878	8.8247	0.89357	0.72792	0.97566
22	26.798	-2.4685	6.181	2.2179	0.89619	0.76084	0.97773
23	27.168	-1.1693	-7.1271	3.4469	0.89678	0.80462	0.98272
24	27.519	-2.2207	-12.988	-4.6328	0.8989	0.95	0.99174
25	27.626	4.5585	-6.8584	-7.59E-02	0.90783	0.99054	0.99174

Continuation of Table 3

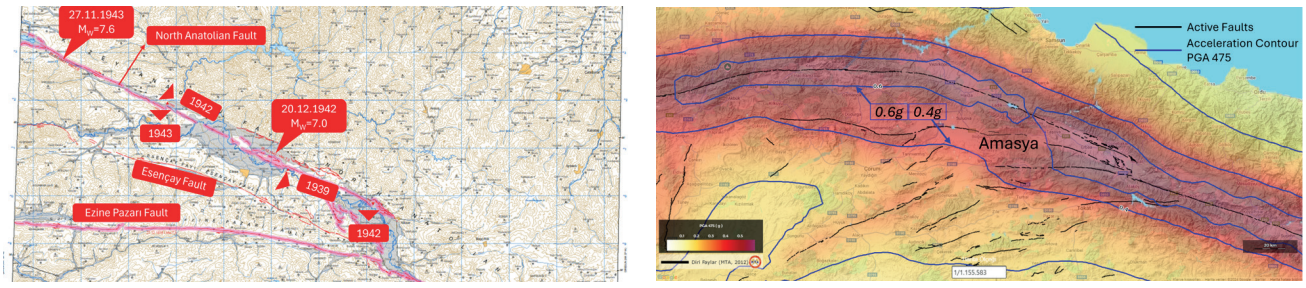
Mode	Frequency (Hz)	Participation factor Directions			Cumulative effective mass fraction Directions		
		X	Y	Z	X	Y	Z
26	28.207	8.5962	0.92166	2.574	0.93958	0.99127	0.99453
27	29.668	3.3682	2.7266	2.9206	0.94446	0.99768	0.99811
28	30.594	10.163	-7.14E-02	-1.7456	0.98884	0.99768	0.99939
29	30.769	-3.9706	1.6149	-0.64022	0.99562	0.99993	0.99956
30	31.16	-3.1939	0.28161	1.0198	1	1	1

3.6 Seismicity of the region

Amasya is located within the east-west trending North Anatolian Fault Zone, an active fault that has generated nine earthquakes of magnitude seven or higher in the past century. Seismic information about city of Amasya can be seen in Fig. 11. The rupture points and active fault lines are shown in Fig. 11(a) [41].

According to the earthquake hazard map of Türkiye, prepared by the Disaster and Emergency Management Presidency (AFAD) for the city of Amasya, the maximum acceleration for a 475-year return period ranges from 0.4 g to 0.6 g (Fig. 11(b)) [10]. Geotechnical investigations in the region have determined that the building site soil consists of firm sand or hardened clay, corresponding to class ZC in TBDY2018 [42].

Four major earthquakes in Türkiye were selected for the nonlinear time-history analyses: the 1992 Erzincan, 1999 Düzce, 2023 Kahramanmaraş-Pazarcık, and 2023 Kahramanmaraş-Elbistan earthquakes. Detailed information on these earthquakes, including the original PGA values of the selected records, is provided in Table 4. It should be emphasized that the PGA values listed in Table 4 correspond to the original recorded motions at their respective recording stations and should not be interpreted as site-specific PGA values for Amasya. The selected acceleration records were subsequently spectrally matched to the site-specific design spectrum using a time-domain wavelet-based procedure [43]. The matching procedure follows the approaches proposed by Hancock et al. [44] and Al Atik and Abrahamson [45], in which localized wavelet adjustments are introduced into the original acceleration time series to achieve spectral compatibility while limiting artificial modification of the temporal characteristics of the ground motion. In particular, the Al Atik and Abrahamson procedure was developed to preserve the nonstationary character of recorded motions during spectral matching. The design spectrum for an earthquake with a 10% probability of exceedance in 50 years and the



(a) (b)

Fig. 11 Seismic information about Amasya (a) Active Faults around Amasya [41]; (b) Seismic intensity map of the region [10]

Table 4 Ground motion details [9]

Earthquake	Code	Event Date	M_w	Depth (km)	Soil Class (EC8)	Epicentral Distance (km)	Original PGA (cm/s^2)	
							E-W Dir.	N-S Dir.
Erzincan	ERZ	13.03.1992	6.6	22.6	B	12.82	479.543	405.007
Düzce	DZC	12.11.1999	7.1	11.0	C	36.12	803.83	719.330
Pazarcik	PZR	06.02.2023	7.7	8.6	B	31.42	2283.77	2089.368
Elbistan	ELB	06.02.2023	7.6	7.0	B	67.00	635.471	522.694

matched response spectra of the selected records are presented in Fig. 12, whereas the original, unmodified acceleration time histories of the selected earthquake records are presented in Fig. 13. Although the adopted wavelet-based procedure is intended to preserve the nonstationary characteristics of the original records, no separate pulse-preservation metric was evaluated for the Pazarcık and Elbistan motions. Therefore, the possible influence of spectral matching on specific near-fault pulse characteristics is acknowledged as a limitation of the present ground-motion processing procedure.

The elastic design spectrum indicates that the structure may experience accelerations exceeding 1.2 g during a potential future earthquake. Given the substantial mass of the structure (3301.83 tons), it is reasonable to assume that the horizontal force acting on the structure during an earthquake will be extremely large.

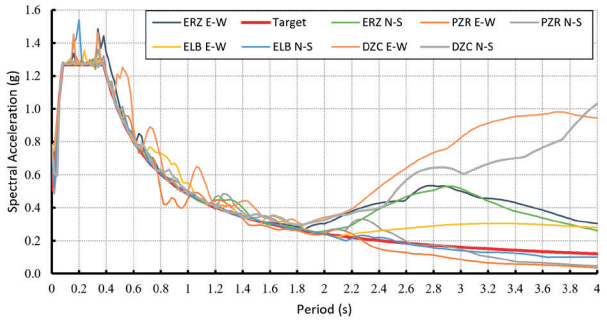
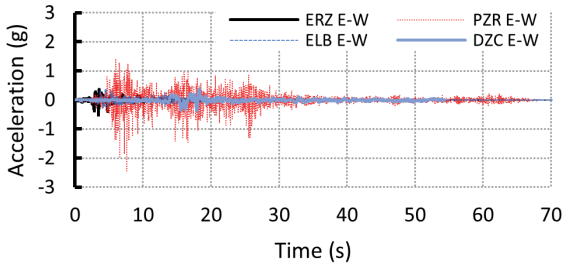
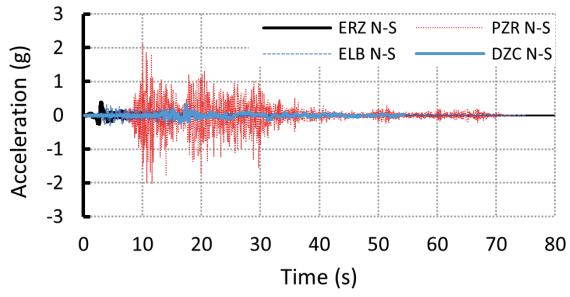


Fig. 12 The target and matched spectra



(a)



(b)

Fig. 13 Original acceleration time histories of the selected earthquake records (a) E-W components of the accelerograms; (b) N-S components of the accelerograms

3.7 Non-linear time-history analysis

To ensure the accuracy and reproducibility of results in finite element analyses, mesh refinement and convergence studies were performed. As mentioned earlier the element type used in the analyses was the SOLID65 element. The initial mesh was defined homogeneously to match the general geometry of the model; local mesh refinement was then applied to regions where stress concentrations were expected (such as arch-slab connections, opening corners, and load transfer regions). The nonlinear time-history analyses were performed using the finite element mesh configuration determined in the mesh sensitivity study described in Section 3.3.

As part of convergence control, automatic time stepping was employed and the residual values of the iterative solution process were monitored at each step. The Newton–Raphson iterations were considered converged when the energy-based convergence tolerance fell below 0.0001. For the 500 mm model used in the principal analyses, the initial, minimum, and maximum time-step sizes were set to 0.001, 0.001, and 0.005 s, respectively. As noted in Section 3.3, the fine-mesh sensitivity analysis required adjusted time-stepping parameters to obtain a stable converged solution.

The base shear–displacement responses obtained from the nonlinear time-history analyses at the dome-tip control points in the X and Z directions are presented in Fig. 14. The structure contains two principal domes covering the Tevhidhane and the Masjid. The dome over the Tevhidhane was designated as the "large dome" because it has a larger radius (r = 9000 mm) than the other dome (r = 8000 mm), which was designated as the "small dome".Because historic masonry does not exhibit a sharply defined global yield point comparable to ductile structural materials, the base-shear level associated with the onset of nonlinear response was identified approximately from the first pronounced departure of the cyclic response from its initial quasi-linear trend. This point reflects the beginning of appreciable stiffness degradation and nonlinear deformation rather than a mathematically exact yield state. Accordingly, the values reported in Table 5 should be interpreted as approximate indicators of the base-shear level at which significant nonlinear response begins. The corresponding base-shear-to-weight ratios were calculated using the total weight of the modeled structural system excluding the minaret. A 5% proportional viscous damping ratio was adopted in all nonlinear time-history analyses.

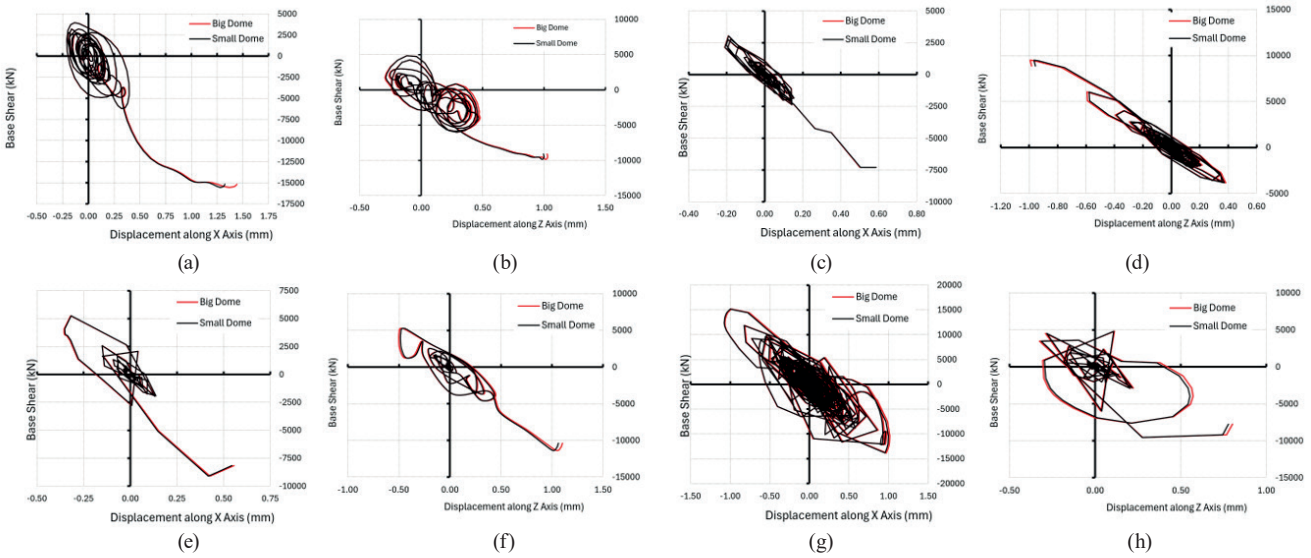


Fig. 14 Base shear–displacement response histories at the dome-tip control points (a) Erzincan earthquake, X direction (East–West); (b) Erzincan earthquake, Z direction (North–South); (c) Düzce earthquake, X direction (East–West); (d) Düzce earthquake, Z direction (North–South); (e) Elbistan earthquake, X direction (East–West); (f) Elbistan earthquake, Z direction (North–South); (g) Pazarcık earthquake, X direction (East–West); (h) Pazarcık earthquake, Z direction (North–South)

Table 5 Base Shear-Total weight ratios

Earthquakes	Total Weight (W) (kN)	Base Shear (V) (kN)		V/W	
		E-W	N-S	E-W	N-S
Erzincan	3.2391×10^4	15000	10000	0.463	0.309
Düzce		7500	9500	0.232	0.293
Pazarcık		15000	9000	0.463	0.278
Elbistan		9000	11000	0.278	0.340

Note: Base Shear denotes the base shear force corresponding to the approximate onset of nonlinear response.

Previous studies on historical masonry structures confirm these ratios. Sözen [40] calculated this ratio as 0.27 in his study of a masonry clock tower, while Brandonisio et al. [46] found it to be between 0.20 and 0.35 in their investigation of the effects of the 2009 L'Aquila earthquake on masonry church structures.

Fig. 15 presents the planar displacement traces of the tips of the large and small domes during the applied ground motions. The displacement trajectories of the two domes remain closely correlated during the initial stage of the response, indicating similar kinematic behavior before the onset of significant nonlinear deformations. As the structure enters the pronounced nonlinear response, however, the trajectories progressively diverge, and a noticeable shift of the displacement reference point becomes evident. This shift indicates the development of residual displacements associated with irreversible deformation and stiffness degradation. The large dome exhibits a slightly wider displacement range, particularly in the negative X direction, compared with the small dome, suggesting a greater deformation demand in the large dome. The increasingly different displacement histories of the two domes after the onset of significant nonlinear response also indicate that their subsequent nonlinear response is no longer fully compatible, reflecting the development of differential deformation within the dome system. Overall, the displacement traces demonstrate that the seismic response evolves from a relatively coordinated deformation pattern in the initial quasi-linear stage to a more complex and asymmetric response governed by plastic deformation and residual displacements.

Fig. 16(a), (c), (e), and (g) present the distribution of the equivalent total strain remaining in the structure at the end of the analyses, whereas Fig. 16(b), (d), (f), and (h) show the maximum equivalent total strain attained during the ground-motion histories. The residual strain distributions indicate that permanent deformation is not uniformly distributed throughout the structure. Higher strain concentrations are mainly observed around the dome–support interfaces, the connecting masonry regions, and the corner zones of the structure. These localized concentrations identify regions subjected to elevated deformation demand and indicate that the geometric and stiffness transitions between the domes and their supporting elements constitute critical regions under seismic loading.

It should be noted that the equivalent total strain contours are used primarily to identify regions of concentrated deformation demand and are not interpreted directly as

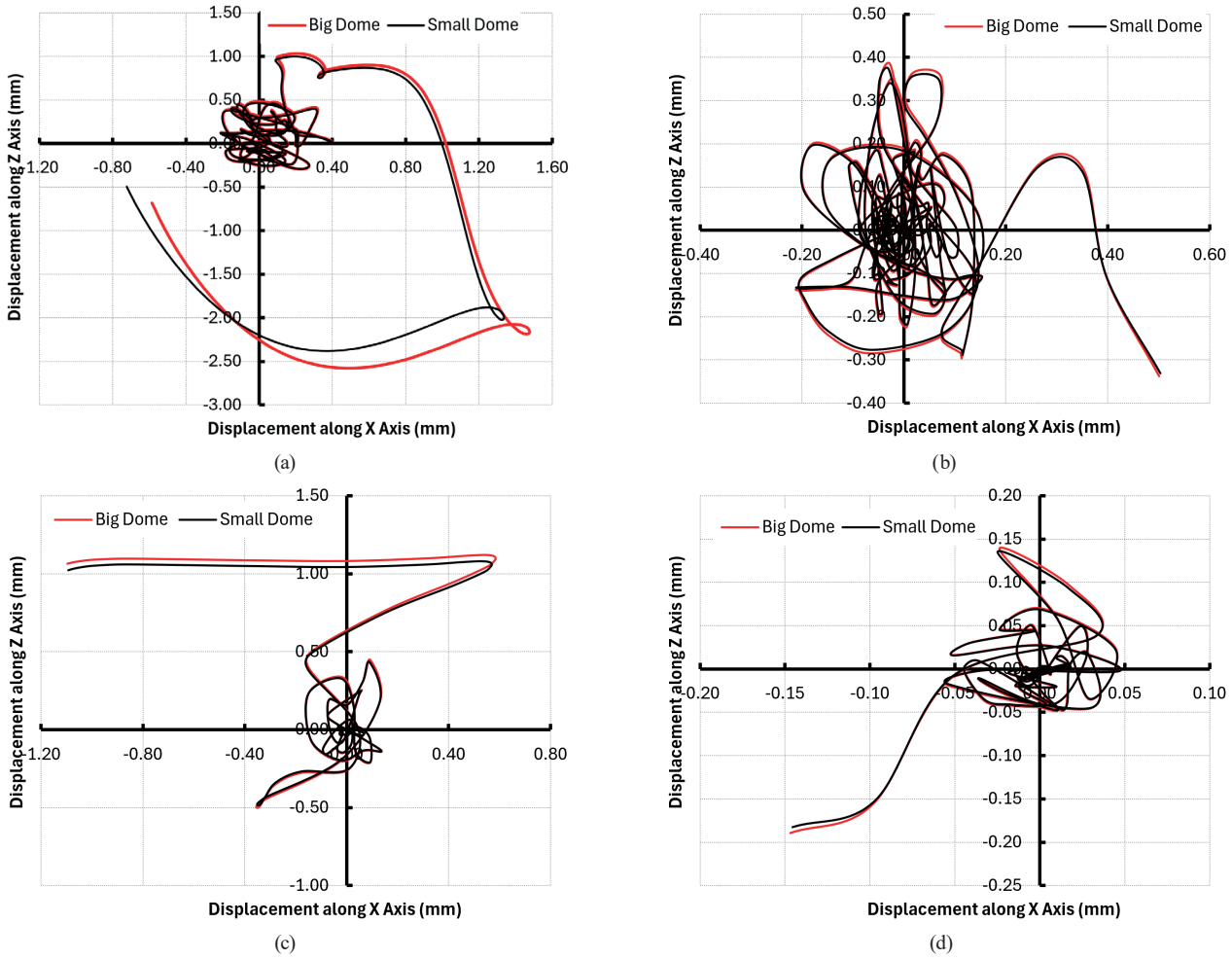


Fig. 15 Traces of planar movement of the peak nodes (a) Erzincan earthquake; (b) Düzce earthquake; (c) Elbistan earthquake; (d) Pazarcık earthquake

a tensile cracking criterion. Damage initiation was evaluated independently by comparing the maximum principal tensile stress with the adopted tensile strength of the masonry, f_t = 0.30 MPa. For reference, the corresponding uniaxial elastic tensile strain calculated from the adopted material properties (f_t = 0.30 MPa and E = 3900 MPa) is approximately 7.66×10^{-4}. However, because the quantity presented in Fig. 16 is equivalent total strain rather than uniaxial tensile strain, this value is not used as a direct contour-based failure threshold. The concentration of strain in the dome–support transition regions is consistent with the differential displacement behavior observed between the large and small domes in Fig. 15, while the occurrence of tensile cracking in the critical regions is assessed separately on the basis of the maximum principal tensile stress exceeding the adopted tensile strength.

The elastic deformation limit was exceeded in the dodecagonal pulleys supporting the domes and in the body walls of the building. The lower parts of the large dome near the southeast-facing pulley are damaged. The south façade wall of the building was severely damaged during the collapse phase. The vaults covering the ordeal rooms, which are connected to the building wall, were also damaged.

For clarity, the numerical analyses employed in the present study, their principal objectives, and the corresponding verification or supporting evidence are summarized in Table 6. This overview also distinguishes the preliminary model-characterization analyses from the nonlinear dynamic analyses used for the seismic vulnerability and damage assessment.

4 Results and discussion

4.1 Seismic damage mechanism and structural vulnerability assessment

This section evaluates the seismic damage mechanisms and structural vulnerability of the Amasya Çilehane Complex based on the nonlinear dynamic analysis results. The numerical findings are compared with damage patterns documented in archival photographs following past earthquakes in order to examine the spatial consistency

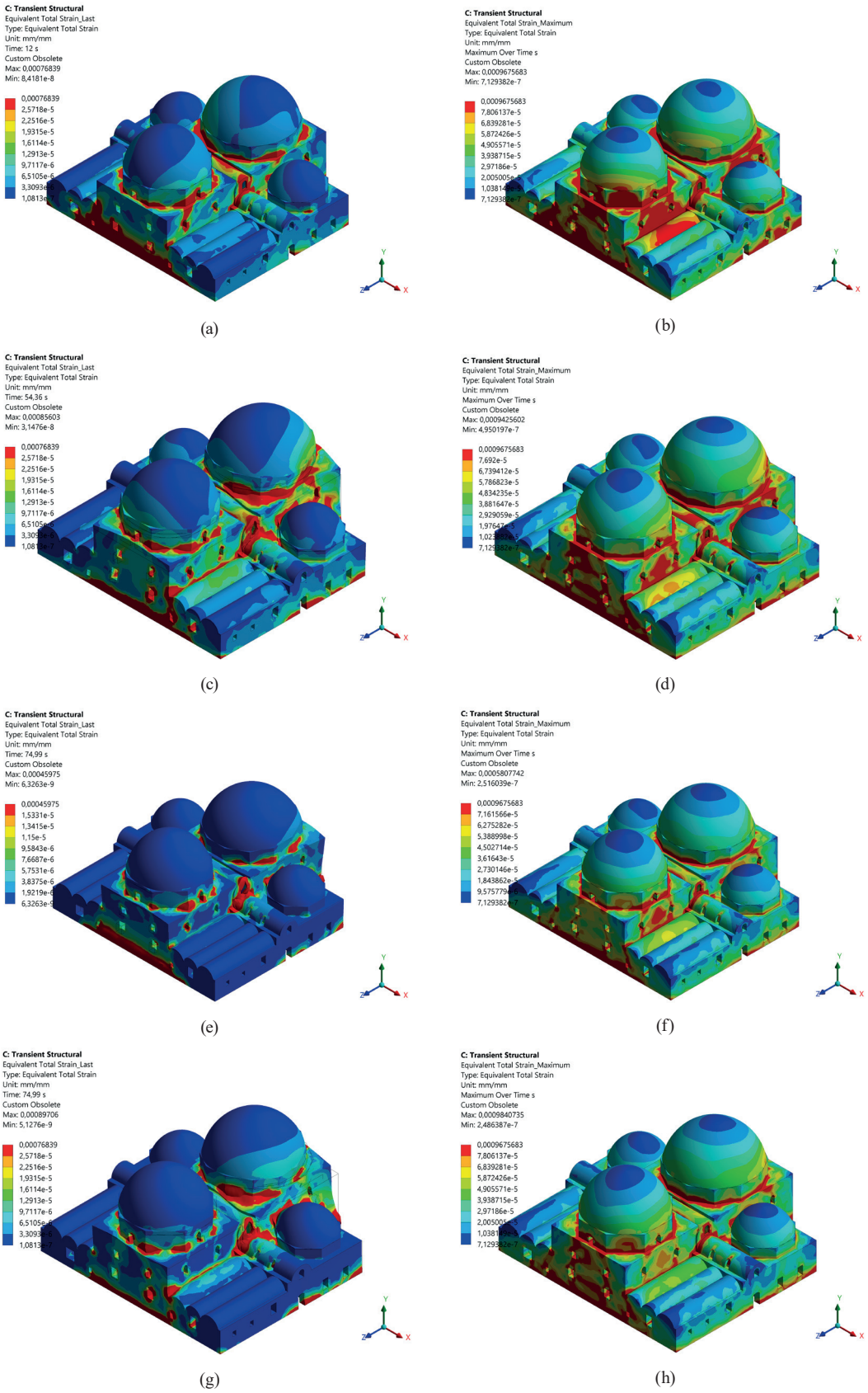


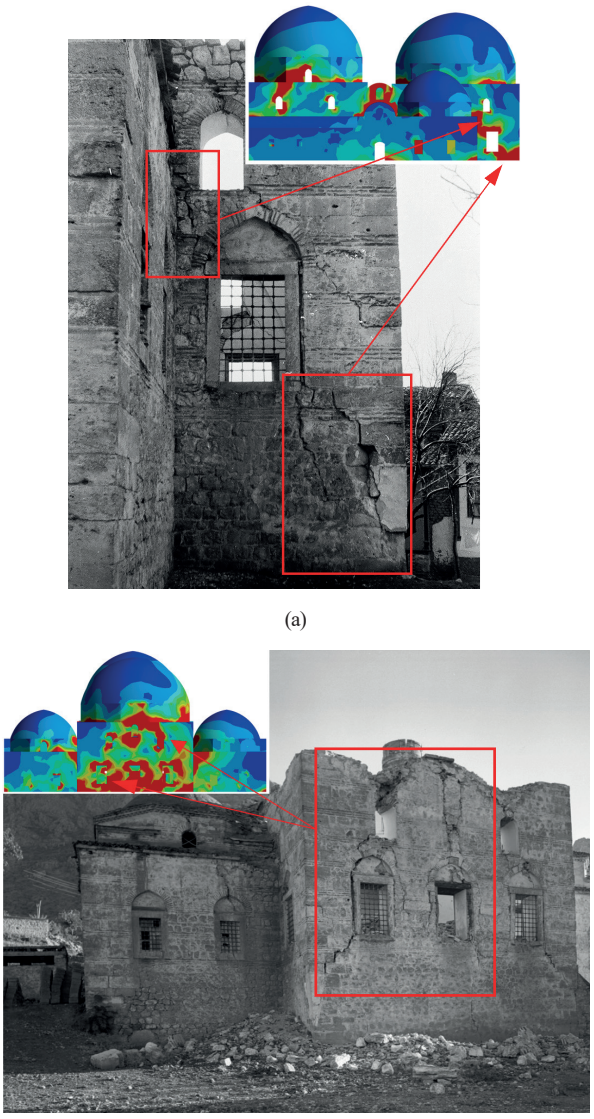
Fig. 16 Strain distribution (a) residual strain after the Erzincan earthquake; (b) maximum strain during the Erzincan earthquake; (c) residual strain after the Düzce earthquake; (d) maximum strain during the Düzce earthquake; (e) residual strain after the Pazarcık earthquake; (f) maximum strain during the Pazarcık earthquake; (g) residual strain after the Elbistan earthquake; (h) maximum strain during the Elbistan earthquake

Table 6 Summary of the numerical analyses and corresponding verification evidence

Analysis stage	Principal purpose	Main response quantities	Verification/supporting evidence
Mesh sensitivity analysis	Assess the influence of mesh density and select an appropriate discretization	Fundamental frequency and mesh-dependent response parameters	Convergence between the medium and fine meshes; supplemented by the nonlinear mesh-sensitivity assessment described in Section 3.3
Nonlinear static analysis under gravity load	Establish the gravity-loaded equilibrium state and identify initial stress/deformation concentrations	Stress distribution, vertical deformation, structural self-weight	Physical consistency of stress and deformation patterns under self-weight
Modal analysis	Characterize the global dynamic properties of the modeled structural system	Natural frequencies, mode shapes, participating mass ratios	Consistency of modal characteristics and cumulative mass participation
Nonlinear time-history analysis	Evaluate seismic demand, nonlinear response, and damage localization under selected earthquake records	Base shear, displacement, drift, tensile-stress exceedance, and strain localization	Spectrum compatibility of the input motions and qualitative spatial comparison between predicted damage zones and historically observed earthquake damage

between the predicted critical regions and the historically observed damage and to identify the dominant failure mechanisms of the structure. Because precise information regarding the date of each photograph and quantitative measurements of the observed cracks are not available, the photographic evidence is used only for qualitative comparison. Figs. 17 and 18 present comparisons between the historically observed damage patterns and the critical regions identified by the nonlinear dynamic analyses. Due to the similarity of the damage patterns obtained from the different ground-motion records considered in the analyses, only the results corresponding to the Erzincan record are presented for this comparison. The correspondence between the locations and orientations of the numerically predicted critical regions and the observed crack patterns provides qualitative corroboration of the predicted damage mechanisms. However, this comparison should not be interpreted as quantitative validation of the numerical model because measured crack widths, deformation records, and structure-specific material data from the historical earthquake events are unavailable.

According to available information, the heavily damaged domes of the complex were demolished and unfortunately replaced by reinforced concrete domes. For this reason, the domes are visible in some photos but not in others. Additionally, the photos show that the minaret, which was not included in the analyses, collapsed above the level of its balcony. The available archival photographs were obtained from different periods, and precise metadata regarding the date of each photograph are not available. Therefore, they are used in the present study to document historically observed damage patterns rather than to reconstruct the response of the complex to a specific earthquake event.



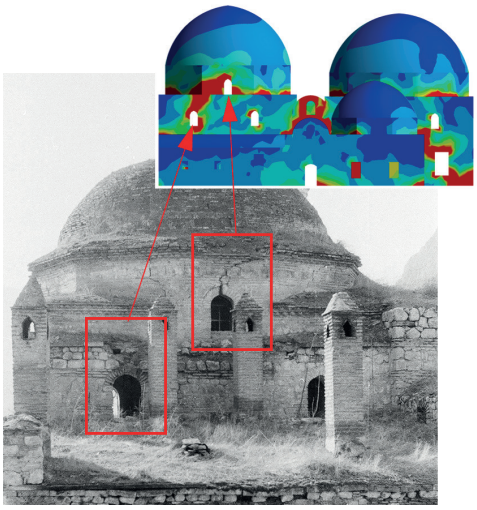
(a)

(b)

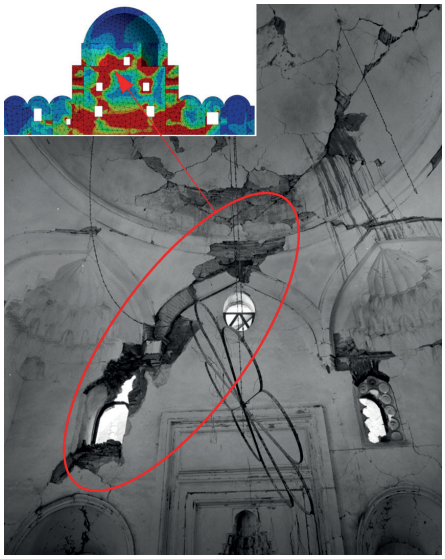
Fig. 17 Shear cracks on façades (a) Large shear cracks of north façade; (b) Large shear cracks of north façade



(a)



(b)



(c)

Fig. 18 Comparison of damage from past earthquakes with analysis results (a) Damage on east façade pulleys; (b) Damage on west façade pulleys; (c) Damages on the interior wall of the south façade

The walls of the north façade of the complex (Fig. 17(a) and Fig. 17(b)) show large shear cracks emanating from the edges of the window openings. The total strain and the maximum principal stress from the analyzes of the damaged wall sections were calculated as 3.95×10^{-4} to 9.67×10^{-4} and 0.32 to 0.35 MPa, respectively.

Similarly, on the east and west facades (Fig. 18(a) and Fig. 18(b)), there is heavy damage on the pulleys supporting the dome. The total strain and the maximum principal stress in the rings supporting the dome were calculated as 2.69×10^{-4} and 0.3287 MPa respectively. It is clear that the calculated strain and stress values exceed the elastic limit. Fig. 18(c) also shows a photograph of the interior of the south façade of the mosque in the complex. It can be seen that the crack extends from the upper edge of the window opening directly above the left side of the mihrab toward the dome. Examination of the total strain distribution obtained from the numerical analyses shows that the elastic strain was exceeded in the same area. The plastic strain in the damaged area was calculated to be 9.69×10^{-5}. The analysis results show that the maximum principal stress in the same area exceeds the tensile strength of the stone, which is 0.30 MPa, and was calculated as 0.32 MPa. The spatial correspondence between the numerically identified critical regions and the historically observed crack locations supports the predicted damage mechanisms at a qualitative level.

The maximum horizontal displacements of the tips of the large dome and the façade walls of the building resulting from the nonlinear numerical analysis are shown in Table 7. In addition, the displacement ratios corresponding to the horizontal displacements and the limit values for immediate occupancy (IO) in three different regulations are given in Table 8 [47, 48, 28].

The calculated drift ratios are significantly lower than the immediate occupancy (IO) limits specified in FEMA 356, ASCE 41, and DGF guidelines. Similar low drift demands have also been reported for historic masonry mosques, which can be attributed to their relatively low center of mass and the high global stiffness provided by thick masonry walls [8, 13, 49]. In addition, the magnitude of the calculated drift response is influenced by the adopted elastic modulus, with relatively high stiffness values generally resulting in lower global deformation demands. Previous studies have also suggested that drift limits specifically adapted to historic masonry structures, including historical mosques, may be more appropriate than the direct application of conventional code-based limits [37, 50].

Table 7 Maximum displacements of structural members

Structural Member	Nodal displacement (mm)							
	Erzincan		Düzce		Pazarcık		Elbistan	
	X Dir.	Z Dir.	X Dir.	Z Dir.	X Dir.	Z Dir.	X Dir.	Z Dir.
Big Dome	1.477	2.580	1.812	1.512	1.067	1.535	1.715	1.464
North façade wall	0.989	2.783	1.380	1.838	0.733	1.578	1.280	1.547
South façade wall	0.712	2.166	0.833	1.599	0.538	1.372	0.778	1.222
East façade wall	0.504	0.762	0.680	0.526	0.405	0.475	0.647	0.437
West façade wall	1.346	1.386	1.400	0.929	0.887	0.819	1.311	0.733

Table 8 Drift ratios of structural members and acceptance criteria in standards

Structural Member	Height (mm)	Drift ratios (%)								Acceptance criteria for IO		
		Erzincan		Düzce		Pazarcık		Elbistan		FEMA356 [47]	ASCE41 [48]	DGF [28]
		X Dir.	Z Dir.	X Dir.	Z Dir.	X Dir.	Z Dir.	X Dir.	Z Dir.			
Big Dome	13560	0.01	0.02	0.01	0.01	0.01	0.01	0.01	0.01	0.10	0.10	0.30
North façade wall	6860	0.01	0.04	0.02	0.03	0.01	0.02	0.02	0.02			
South façade wall	6860	0.01	0.03	0.01	0.02	0.01	0.02	0.01	0.02			
East façade wall	6860	0.01	0.01	0.01	0.01	0.01	0.01	0.01	0.01			
West façade wall	6860	0.02	0.02	0.02	0.01	0.01	0.01	0.02	0.01			

However, the low global drift demand observed in the analyses does not necessarily imply a low level of local damage. Historic masonry structures are characterized by limited tensile capacity and brittle cracking mechanisms, and therefore significant localized damage may develop even when the overall structural deformation remains small. In the present analyses, tensile stress concentrations around façade openings, dome–support transition zones, and interior masonry walls locally exceed the adopted tensile strength of the masonry despite the relatively small global drift ratios. To quantify this local response, a tensile demand ratio, $\eta_t = \sigma_{1,\max}/f_t$, was used, where $\sigma_{1,\max}$ is the maximum principal tensile stress and f_t = 0.30 MPa is the adopted tensile strength of the masonry. Values of $\eta_t \geq 1$ indicate that the tensile strength has been exceeded and that tensile cracking is expected according to the adopted constitutive model. As summarized in Table 9 the representative critical regions identified by the analyses, η_t ranges approximately from 1.07 to 1.17, confirming local tensile-strength exceedance even though the corresponding global drift ratios remain below the immediate-occupancy limits.

These results demonstrate that global displacement-based indicators alone are insufficient to characterize the seismic vulnerability of the Çilehane Complex. The drift ratios should therefore be interpreted together with local tensile-strength exceedance, residual strain concentrations, and the spatial distribution of the numerically identified critical regions. This combined assessment is particularly important for historic masonry structures, in which brittle cracking and localized failure may develop before substantial global deformation occurs.

4.2 Implications for retrofitting strategies

The nonlinear dynamic analyses identified diagonal shear cracking in the façade walls and tensile stress concentrations around the vault–dome transition zones as the dominant seismic damage mechanisms of the complex. These

Table 9 Local tensile demand ratios in representative critical regions for the Erzincan ground-motion record

Critical region	$\sigma_{1,\max}$ (MPa)	f_t (MPa)	$\eta_t = \sigma_{1,\max}/f_t$	Assessment
North façade around window openings	0.32–0.35	0.30	1.07–1.17	Tensile strength exceeded
Dome-support transition zone	0.3287	0.30	1.10	Tensile strength exceeded
Interior wall of the south façade	0.32	0.30	1.07	Tensile strength exceeded

Note: $\eta_t \geq 1.0$ indicates that the local maximum principal tensile stress exceeds the adopted tensile strength of the masonry.

findings indicate that any future strengthening study should primarily address the limited in-plane shear resistance of the façade walls and the localized tensile vulnerability of the dome-supporting regions, while avoiding substantial changes in the mass, stiffness distribution, and architectural character of the monument.

The present analyses, however, were performed exclusively for the existing unstrengthened structure and therefore do not provide a quantitative assessment of the effectiveness of any specific retrofit technique. Accordingly, the findings should be interpreted primarily as a basis for identifying critical structural regions and defining the mechanical objectives of possible future interventions, rather than as analytically validated recommendations for a particular strengthening system. The selection of an appropriate intervention technique would require consideration of structural effectiveness together with material compatibility, reversibility, durability, anchorage requirements, and conservation constraints. Future studies should explicitly model selected conservation-compatible strengthening configurations and evaluate their influence on stress redistribution, displacement demand, damage localization, and overall seismic response before any specific intervention is recommended.

4.3 Modelling assumption and study limitations

The nonlinear finite element model was developed under several simplifying assumptions that should be acknowledged when interpreting the results. Soil–structure interaction (SSI) was not explicitly incorporated because detailed site-specific geotechnical parameters and reliable information on the existing foundation system were not available; consequently, fixed-base boundary conditions were adopted. This assumption implies that the reported modal properties, displacement demands, base-shear response, and local stress concentrations represent the response of the superstructure under a fixed-support idealization. In reality, foundation and soil flexibility may modify the effective dynamic characteristics of the system through period elongation, foundation rocking and translation, and redistribution of seismic demands. Depending on the relative stiffness of the soil–foundation-structure system, these effects may either increase or reduce local and global response quantities. Therefore, the influence of SSI on the calculated displacement demands and damage localization remains a source of modelling uncertainty in the present study. A rigorous assessment of this effect would require site-specific soil stiffness, damping, foundation geometry, and soil–foundation interface information, which were not available for the present investigation.

Previous studies have shown that uncertainties in elastic modulus, tensile strength, and boundary conditions can influence displacement demands, capacity estimates, and even collapse mechanisms by altering modal properties and stress localization. Minor architectural and ornamental elements were excluded from the numerical model because their contribution to the global structural response was considered negligible. The minaret, however, was treated separately and was excluded because the present study focuses on the seismic response and damage mechanisms of the main masonry complex. Consequently, the reported modal participation, structural weight, base-shear response, and damage patterns correspond to the modeled main structural system excluding the minaret. Historical photographs indicate that the minaret experienced severe local damage and collapse above the balcony level, demonstrating its considerable seismic vulnerability. Nevertheless, because a coupled model including the minaret was not analyzed, its possible influence on the mass and stiffness distribution of the complete monument cannot be quantified within the present study and is therefore acknowledged as an additional modelling limitation.

Direct experimental validation could not be performed because the structure is a protected historical monument and regulatory permissions for material sampling or in-situ dynamic testing were not available. Therefore, the comparison between the numerical results and the archival earthquake-damage photographs was used solely as qualitative corroboration of the predicted damage mechanisms. In particular, the comparison evaluates the spatial consistency between the numerically identified critical regions and the historically documented damage locations; it does not constitute quantitative validation or calibration of the finite element model because measured crack widths, displacement records, and structure-specific mechanical properties from the historical earthquake events are unavailable. A comprehensive material-parameter sensitivity and probabilistic uncertainty analysis was also beyond the scope of the present study. Although the adopted material properties and damping ratio were selected from values reported for comparable historic masonry typologies, their uncertainty may influence quantitative stress, strain, and displacement predictions. Future studies should therefore incorporate structure-specific material characterization, parametric and probabilistic uncertainty analyses, site-specific geotechnical investigations, and an explicit soil–foundation model. Within these limitations, the observed spatial consistency between the numerically predicted critical regions and the documented

earthquake-damage patterns provides qualitative support for the identified dominant damage mechanisms, without implying quantitative validation of the adopted model parameters or predicted response amplitudes.

5 Conclusions

The nonlinear finite element analyses performed for the Amasya Çilehane Complex indicate a high seismic vulnerability under design-level earthquake scenarios. The results demonstrate that, for an earthquake with a 10% probability of exceedance in 50 years, the structural system is expected to experience severe damage, with a significant risk of partial or global collapse. The dominant damage mechanisms are characterized by diagonal shear cracking in the east–west and north–south façade walls, accompanied by substantial stress concentrations in the vaults supporting the domes and in interior masonry walls. These findings reveal critical weaknesses in the in-plane shear capacity and tensile resistance of the masonry system. Based on the identified damage patterns and structural response characteristics, the results indicate the need for a detailed evaluation of conservation-compatible seismic strengthening alternatives for the long-term preservation of the complex. The analytical framework presented in this study provides a rational basis for identifying critical structural regions and for guiding future studies in which specific retrofit configurations can be explicitly modeled and evaluated.

References

[1] Bayraktar, A., Şahin, A., Özcan, D. M., Yildirim, F. "Numerical damage assessment of Haghia Sophia bell tower by nonlinear FE modeling", Applied Mathematical Modelling, 34(1), pp. 92–121, 2010. https://doi.org/10.1016/j.apm.2009.03.033

[2] Milani, G., Casolo, S., Naliato, A., Tralli, A. "Seismic Assessment of a Medieval Masonry Tower in Northern Italy by Limit, Nonlinear Static, and Full Dynamic Analyses", International Journal of Architectural Heritage, 6(5), pp. 489–524, 2012. https://doi.org/10.1080/15583058.2011.588987

[3] D'Altri, A.M., Sarhosis, V., Milani, G., Rots, J., Cattari, S., Lagomarsino, S., Sacco, E., Tralli, A., Castellazzi, G., de Miranda, S. "Modeling strategies for the computational analysis of unreinforced masonry structures: Review and classification", Archives of Computational Methods in Engineering, 27, pp. 1153–1185, 2020. https://doi.org/10.1007/s11831-019-09351-x

[4] Cakir, F., Uckan, E., Shen, J., Seker, B. S., Akbas, B. "Seismic damage evaluation of historical structures during Van earthquake, October 23, 2011", Engineering Failure Analysis, 58(1), pp. 249–266, 2015. https://doi.org/10.1016/j.engfailanal.2015.08.030

[5] Koseoglu, G. C., Canbay, E. "Assessment and rehabilitation of the damaged historic Cenabı Ahmet Pasha Mosque", Engineering Failure Analysis, 57, pp. 389–398, 2015. https://doi.org/10.1016/j.engfailanal.2015.08.015

[6] Şentürk, İ., Ergün, M., Artar, M. "Seismic behavior assessment of historical Alaeddin Bey Mosque and strengthening suggestions by CFRP fabric and steel plate", Engineering Failure Analysis, 137, 106242, 2022. https://doi.org/10.1016/j.engfailanal.2022.106242

[7] Kocaman, İ., Kazaz, İ. "Collapse mechanism of historical masonry mosques under strong ground motions", Engineering Failure Analysis, 144, 106983, 2023. https://doi.org/10.1016/j.engfailanal.2022.106983

[8] Cakir, F., Odabas, A., Zulfikar, A. C., Zeyrek, S., Kir, G. "Structural performance assessment before strengthening of historic Structures: A case study of the historical Şerafettin mosque in Turkey", Engineering Failure Analysis, 153, 107532, 2023. https://doi.org/10.1016/j.engfailanal.2023.107532

[9] Directorate of Diaster and Emergency Management (DDEM) "1900-20XX Earthquake Catalog (M>=4)", Disaster and Emergency Management Authority. [online] Available at: https://deprem.afad.gov.tr/depremkatalogu# [Accessed: 1 June 2024]

[10] AFAD "Earthquake Hazard Maps Interactive Web Applications", Disaster and Emergency Management Authority. [online] Available at: https://tdth.afad.gov.tr/TDTH/main.xhtml [Accessed: 1 June 2024]

[11] Kazaz, İ., Gülkan, P., Kazaz, E. "Numerical assessment of cracks on a freestanding masonry minaret", International Journal of Architectural Heritage, 15(4), pp. 526–547, 2021. https://doi.org/10.1080/15583058.2019.1629046

[12] Vitorino, S., Corazzi, R., Doz, G. "Seismic performance assessment of the historical Cathedral of Santa Maria del Fiore Dome by numerical analysis", Engineering Failure Analysis, 165, 108734, 2024. https://doi.org/10.1016/j.engfailanal.2024.108734

[13] Kocaman, İ., Kazaz, İ. "Tarihi bir caminin hasar sınırlarının irdelenmesi, Konya Sultan Selim Cami örneği (Examination of the damage limits of a historical mosque, Konya Sultan Selim Mosque example)", Gazi Üniversitesi Mühendislik Mimarlık Fakültesi Dergisi, 39(1), pp. 51–64, 2024. https://doi.org/10.17341/gazimmfd.1161378 [in Turkish]

[14] Dedeoğlu, İ. Ö., Yetkin, M., Calayır, Y. "Seismic performance of masonry structures in the rural area during the November 23, 2022, Düzce-Gölyaka earthquake", Journal of Building Engineering, 96, 110373, 2024. https://doi.org/10.1016/j.jobe.2024.110373

[15] Shabani, A., Kioumarsi, M., Plevris, V. "Performance-based seismic assessment of a historical masonry arch bridge: Effect of pulse-like excitations", Frontiers of Structural and Civil Engineering, 17(6), pp. 855–869, 2023. https://doi.org/10.1007/s11709-023-0972-z

[16] Gonçalves, M., Ponte, M., Bento, R. "Seismic Assessment of Existing Masonry Buildings Using Damage Mechanics", Buildings, 14(8), 2395, 2024. https://doi.org/10.3390/buildings14082395

[17] Onat, O., Özmen, A., Özdemir, E., Sayın, E. "Damage propagation and failure mechanism of single dome historical Masonry Mosque after February 6, 2023, Kahramanmaraş earthquake doublets (Mw= 7.7 and Mw= 7.6)", Structures, 69, 107288, 2024. https://doi.org/10.1016/j.istruc.2024.107288

[18] Lagomarsino, S., Penna, A., Galasco, A., Cattari, S. "TREMURI program: An equivalent frame model for the nonlinear seismic analysis of masonry buildings", Engineering Structures, 56, pp. 1787–1799, 2013. https://doi.org/10.1016/j.engstruct.2013.08.002

[19] Lourenço, P. B. "Computations on historic masonry structures", Progress in Structural Engineering and Materials, 4(3), pp. 301–319, 2002. https://doi.org/10.1002/pse.120

[20] Nakashima, M. "Hybrid simulation: An early history", Earthquake Engineering & Structural Dynamics, 49(10), pp. 949–962, 2020. https://doi.org/10.1002/eqe.3274

[21] Rota, M., Penna, A., Magenes, G. "A methodology for deriving analytical fragility curves for masonry buildings based on stochastic nonlinear analyses", Engineering Structures, 32(5), pp. 1312–1323, 2010. https://doi.org/10.1016/j.engstruct.2010.01.009

[22] Türkiye Kültür Portal "Çilehane Camii - Amasya" [online] Available at: https://www.kulturportali.gov.tr/turkiye/amasya/gezilecekyer/clehane-cam [Accessed: 02 September 2024]

[23] Discover Amasya "Çilehane" [online] Available at: https://discoveramasya.com/icerik/74 [Accessed: 11 September 2024]

[24] Decret, D., Malecot, Y., Sieffert, Y., Vieux-Champagne, F., Daudeville, L. "A New Macro-Element for Predicting the Behavior of Masonry Structures under In-Plane Cyclic Loading", Buildings, 14(3), 768, 2024. https://doi.org/10.3390/buildings14030768

[25] Prosperi, A., Longo, M., Korswagen, P. A., Giardina, G., Rots, J. G. "Comparative study of NLFE models for simulating settlement-induced damage in masonry façades: macro-and simplified micro-models", Frontiers in Built Environment, 11, 1618329, 2025. https://doi.org/10.3389/fbuil.2025.1618329

[26] Ansys Inc. "Ansys Mechanical, (Release 2020.2)", [computer program] Available at: https://www.ansys.com/ [Accessed: 25 November 2021]

[27] SolidWorks "SOLIDWORKS, (2020)", [computer program] Available at: https://www.solidworks.com/ [Accessed: 15 May 2021]

[28] DGF "Guidelines for the Management of Earthquake Risks for Historic Buildings", Directorate General of Foundations, Ankara, Türkiye. 2017

[29] Dogangun, A., Sezen, H. "Seismic vulnerability and preservation of historical masonry monumental structures", Earthquake and Structures, 3(1), pp. 83–95, 2012. https://doi.org/10.12989/eas.2012.3.1.083

[30] William, K. J., Warnke, E. P. "Constitutive model for the triaxial behaviour of concrete", Proceedings of the International Association for Bridge and Structural Engineering, 19, pp. 1–30, 1975. https://doi.org/10.5169/seals-17526

[31] Lourenço, P. B. "Computational strategies for masonry structures", PhD Thesis, Universidade do Porto, Porto, Portugal, 1997.

[32] Milani, G., Lourenço, P. B., Tralli, A. "Homogenised limit analysis of masonry walls, Part I: Failure surfaces", Computers & Structures, 84(3–4), pp. 166–180, 2006. https://doi.org/10.1016/j.compstruc.2005.09.005

[33] Peña, F., Lourenço, P. B., Mendes, N., Oliveira, D. V. "Numerical models for the seismic assessment of an old masonry tower", Engineering Structures, 32(5), pp. 1466–1478, 2010. https://doi.org/10.1016/j.engstruct.2010.01.027

[34] Aşıkoğlu, A., D'Anna, J., Ramirez, R., Solarino, F., Romanazzi, A., Ciocci, M. P., Bianchini, N. "Simulation of blind pre-diction and post-diction shaking table tests on a masonry building aggregate using a continuum modelling approach", Bulletin of Earthquake Engineering, 22(12), pp. 6163–6193, 2024. https://doi.org/10.1007/s10518-023-01666-2

[35] Bianchini, N., Ciocci, M. P, Solarino, F., Romanazzi, A., Ramirez, R., D"Anna, J., Aşıkoğlu, A. "Influence of wall-to-floor connections and pounding on pre-and post-diction simulations of a masonry building aggregate tested on a shaking table", Bulletin of Earthquake Engineering, 22(12), pp. 6141–6161, 2024. https://doi.org/10.1007/s10518-023-01641-x

[36] Xie, Q., Xu, D., Zhang, Y., Yu, Y., Hao, W. "Shaking table testing and numerical simulation of the seismic response of a typical China ancient masonry tower", Bulletin of Earthquake Engineering, 18(1), pp. 331–355, 2020. https://doi.org/10.1007/s10518-019-00731-z

[37] Altunişik, A. C., Sunca, F., Genç, A. F., Tavşan, C. "Post-Earthquake Damage Assessments of Historic Mosques and Effects of Near-Fault and Far-Fault Ground Motions on Seismic Responses", International Journal of Architectural Heritage, 17(7), pp. 1043–1078, 2023. https://doi.org/10.1080/15583058.2021.2011475

[38] Aşıkoğlu, A., Avşar, Ö., Lourenço, P. B., Silva, L. C. "Effectiveness of seismic retrofitting of a historical masonry structure: Kütahya Kurşunlu Mosque, Turkey", Bulletin of Earthquake Engineering, 17, pp. 3365–3395, 2019. https://doi.org/10.1007/s10518-019-00603-6

[39] Portioli, F., Mammana, O., Landolfo, R., Mazzolani, F. M., Krstevska, L., Tashkov, L., Gramatikov, K. "Seismic retrofitting of Mustafa Pasha Mosque in Skopje: finite element analysis", Journal of Earthquake Engineering, 15(4), pp. 620–639, 2011. https://doi.org/10.1080/13632469.2010.532580

[40] Sözen, Ş. "Assessment of Seismic Load Capacity of a Slender Masonry Clock Tower", Periodica Polytechnica Civil Engineering, 66(2), pp. 491–501, 2022. https://doi.org/10.3311/PPci.19670

[41] Maden Tetkik ve Arama Genel Müdürlüğü "GeoScience Map Viewer and Drawing Editor" [online] Available at: http://yerbilimleri.mta.gov.tr/anasayfa.aspx [Accessed: 27 January 2021]

[42] TSC "Türkiye Building Seismic Code, TBDY 2018", Disaster and Emergency Management Authority (AFAD), Ankara, Turkey, 2019.

[43] SeismoSoft "Earthquake and Engineering Software Solutions, (2021)", [computer program] Available at: https://seismosoft.com/ [Accessed: 15 November 2025]

[44] Hancock, J., Watson-Lamprey, J., Abrahamson, N. A., Bommer, J. J., Markatis, A., McCoy, E., Mendis, R. "An improved method of matching response spectra of recorded earthquake ground motion using wavelets", Journal of Earthquake Engineering, 10(sup001), pp. 67–89, 2006. https://doi.org/10.1080/13632460609350629

[45] Al Atik, L., Abrahamson, N. "An improved method for nonstationary spectral matching", Earthquake Spectra, 26(3), pp. 601–617, 2010. https://doi.org/10.1193/1.3459159

[46] Brandonisio, G., Lucibello, G., Mele, E., De Luca, A. "Damage and performance evaluation of masonry churches in the 2009 L'Aquila earthquake", Engineering Failure Analysis, 34, pp. 693–714, 2013. https://doi.org/10.1016/j.engfailanal.2013.01.021

[47] Federal Emergency Management Agency "Prestandard and Commentary for the Seismic rehabilitation of Buildings", FEMA 356, Federal Emergency Management Agency, Washington, D.C., 2000

[48] American Society of Civil Engineers "Seismic Evaluation and Retrofit of Existing Buildings", American Society of Civil Engineers, ASCE 41-17, Reston, VA, 2017 https://doi.org/10.1061/9780784414859

[49] Marino, S., Cattari, S., Lagomarsino, S., Ingham, J. M., Dizhur, D. "Modelling of two damaged unreinforced masonry buildings following the Canterbury earthquakes", In: NZSEE Conference, Christchurch, New Zealand, 2016, pp. 1–10. [PDF] Available at: https://www.nzsee.org.nz/db/2016/Papers/O-03%20Marino.pdf [Accessed: 12 November 2026]

[50] Kocaman, I., Kazaz, I., Kazaz, E. "Seismic load capacity of historical masonry mosques by rigid body kinetics", International Journal of Architectural Heritage, 14(6), pp. 849–869, 2020. https://doi.org/10.1080/15583058.2019.1570389